Multichannel Dissociation in Resonant Photoionization of H_2

I. Sánchez and F. Martín

Departamento de Química, C-9, Universidad Autónoma de Madrid, 28049-Madrid, Spain

(Received 5 January 1999)

We present *ab initio* calculations of resonant photoionization of H_2 in the photon energy range 30–37 eV where several ionization and dissociation channels are open. Our results show that the various peaks observed in the spectra are due to the lowest $Q_2\ ^1\Pi_u$ doubly excited state which decays following both a direct and a multistep mechanism. This leads to a reassignment of the resonance structures found in previous experiments. [S0031-9007(99)09069-9]

PACS numbers: 33.80.Eh, 33.80.Gj

Molecular photoionization is currently used to probe electronic and vibrational continua of simple diatomic molecules. In the case of H_2, absorption of photons with energy $\hbar\omega > 18.1$ eV leads to emission of an electron and to dissociation of the molecule according to the equation: $H_2 + \hbar\omega \rightarrow H + H^+ + e^-$. The latter process is called dissociative photoionization and plays a fundamental role in interstellar clouds, planetary atmospheres, and plasma physics. The first experimental evidence of resonant effects was provided by Strathdee and Browning [1] who observed a significant enhancement of the proton production rates at 26.9 and 30.5 eV. This enhancement was immediately related to the existence of doubly excited states lying above the $^2\Sigma_g^+(1s\sigma_g)$ ionization threshold [1,2], in particular, the lowest $Q_1\ ^1\Sigma_u^+$ state (see Fig. 1). Subsequent experiments in this energy region [3,4] revealed additional features that the theory has not been able to explain until very recently [5].

For $\hbar\omega > 30$ eV, the situation is more complicated because several ionization channels are open (see Fig. 1). Furthermore, the Q_2 doubly excited states, which lie above the $^2\Sigma_u^+(2p\sigma_u)$ threshold, are also accessible and may autoionize leading to H_2^+ in the $^2\Sigma_g^+(1s\sigma_g)$ and $^2\Sigma_u^+(2p\sigma_u)$ states. This energy region has been explored in two recent experiments [4,6] by measuring the kinetic energy distribution (KED) of ejected protons.

Our knowledge of multichannel ionization and dissociation in molecular photophysics is practically limited to the above experimental works. No theoretical attempt has been made to model or predict the molecular behavior when dissociation occurs above several ionization thresholds. In this Letter we report the first *ab initio* calculations of KED spectra produced in dissociative photoionization of H_2 in the energy range 30–37 eV and discuss the origin of the resonance structures observed in the experiments. We will conclude that multichannel dissociation through a single doubly excited state leads, in general, to multifeatured spectra that can be interpreted in terms of two different mechanisms.

The theoretical method is inspired in the ideas of [7] and [8], and is a simple generalization of the one used in [5] for the special case of a single ionization channel. It makes use of *B*-spline functions [9] to represent both the electronic and the nuclear wave functions. This allows one to use algebraic techniques in solving the systems of coupled equations that include the interference between the various ionization and dissociation channels. In the dipole approximation, the cross section for ionization from the initial state $\Psi_{g\nu}(\mathbf{r}, R)$ is given (in atomic units) by

$$\sigma_{\alpha v_\alpha}(E) = \frac{4\pi^2\omega}{3c} \sum_{p l_\alpha m} \left| \int dR \times \langle \Psi_{g\nu} | \mathbf{e}_p \cdot \mathbf{D} | \Psi^+_{\alpha v_\alpha l_\alpha m E} \rangle \right|^2 , \quad (1)$$

where g and ν indicate the initial electronic and vibrational states, respectively, $\hbar\omega$ is the photon energy, $\mathbf{e}_p$ is the photon polarization vector, $\mathbf{D}$ is $\mathbf{r}_1 + \mathbf{r}_2$ (length gauge), and $\Psi^+_{\alpha v_\alpha l_\alpha m E}(\mathbf{r}, R)$ is the final state. In the latter state, the superscript + indicates the usual outgoing boundary conditions in electron-molecule scattering, l_α and m are the angular momentum quantum numbers of the ejected electron, $E = W_{g\nu} + \hbar\omega$ with $W_{g\nu}$ the total energy of the molecule in the initial state, and α and v_α denote, respectively, the electronic and vibrational states of the residual molecular ion. In this Letter, α stands for the $^2\Sigma_g^+(1s\sigma_g)$ and $^2\Sigma_u^+(2p\sigma_u)$ states of H_2^+. The label **r**

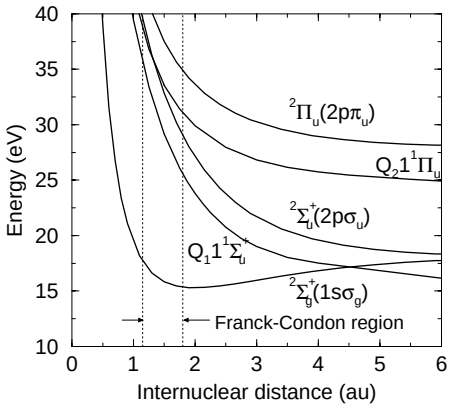

FIG. 1. Potential energy curves of H_2 and H_2^+.

is used for electronic coordinates and R is the internuclear distance. In Eq. (1) we have factored out the rotational wave functions and averaged upon all possible orientations. The initial state is described in the framework of the Born-Oppenheimer (BO) approximation, i.e., $\Psi_{g\nu}(\mathbf{r},R) = \psi_g(\mathbf{r},R)\chi_\nu(R)$, where ψ_g is the $X\,^1\Sigma_g^+$ electronic state of H_2 and χ_ν is the lowest vibrational state calculated in the potential energy curve $E_g(R)$ associated with ψ_g. The dipole selection rule implies that only $^1\Sigma_u^+$ and $^1\Pi_u$ electronic states are populated.

We call ϵ_α the kinetic energy of the outgoing electron in channel α, $\phi_r(\mathbf{r},R)$ the resonant electronic states of energy $E_r(R)$, and $\psi^{0+}_{\alpha l_\alpha m \epsilon_\alpha}(\mathbf{r},R)$ the nonresonant electronic continuum states in which the former are embedded. Then the final state wave function is written [5]

$$\Psi^+_{\alpha v_\alpha l_\alpha E}(\mathbf{r},R) = \sum_{r'} \phi_{r'}(\mathbf{r},R)\xi^{r'}_{\alpha v_\alpha l_\alpha E}(R) + \psi^{0+}_{\alpha l_\alpha \epsilon_\alpha}(\mathbf{r},R)\chi_{v_\alpha}(R) + \lim_{\eta\to 0}\sum_{r'}\sum_{\alpha' l'_{\alpha'}}\sum_{v'_{\alpha'}} dE' \frac{1}{E - E' + i\eta}\int dR'\, V^{r'*}_{\alpha' v'_{\alpha'} l'_{\alpha'} E'}(R')\xi^{r'}_{\alpha v_\alpha l_\alpha E}(R')\psi^{0+}_{\alpha' l'_{\alpha'} \epsilon'_{\alpha'}}(\mathbf{r},R)\chi_{v'_{\alpha'}}(R), \quad (2)$$

where

$$V^r_{\alpha v_\alpha l_\alpha E}(R) = \langle \phi_r | \mathcal{H}_{\rm el} | \psi^{0+}_{\alpha l_\alpha \epsilon_\alpha}\rangle \chi_{v_\alpha}(R) \quad (3)$$

and $\mathcal{H}_{\rm el}$ is the electronic Hamiltonian. Note that we have dropped the index m because $^1\Sigma_u^+$ and $^1\Pi_u$ continuum states, which have different m, are not coupled. In Eqs. (2) and (3), χ_{v_α} is the nuclear wave function solution of

$$[T(R) + E_\alpha(R) - W_{v_\alpha}]\chi_{v_\alpha}(R) = 0, \quad (4)$$

where T is the relative kinetic energy of the nuclei, $E_\alpha(R)$ is the potential energy curve of the α state of H_2^+, W_{v_α} is the energy of the residual H_2^+ ion, $E = \epsilon_\alpha + W_{v_\alpha}$, and $\xi^r_{\alpha v_\alpha l_\alpha E}$ is the solution of [5,7,8]

$$[E - E_r(R) - T(R)]\xi^r_{\alpha v_\alpha l_\alpha E}(R) = V^r_{\alpha v_\alpha l_\alpha E}(R) + \lim_{\eta\to 0}\sum_{r'}\sum_{\alpha' l'_{\alpha'}}\sum_{v'_{\alpha'}} dE' \frac{V^r_{\alpha' v'_{\alpha'} l'_{\alpha'} E'}(R)}{E - E' + i\eta}\int dR'\, V^{r'*}_{\alpha' v'_{\alpha'} l'_{\alpha'} E'}(R')\xi^{r'}_{\alpha v_\alpha l_\alpha E}(R'). \quad (5)$$

The latter equation represents the nuclear motion when the electrons are in the quasistationary state ϕ_r. Equations (2) and (5) are exact within the BO approximation [5,8]. The matrix element in Eq. (3) represents the coupling between the resonance ϕ_r and the nonresonant wave function $\psi^{0+}_{\alpha l_\alpha \epsilon_\alpha}$ and vibrational state χ_{v_α}. Hence, the two terms in the right-hand side of Eq. (5) are the result of the autoionizing character of the ϕ_r state. In particular, the last term represents the decay of the resonant state to the adjacent electronic continuum. This term, as well as the last one in Eq. (2), is nonlocal due to the presence of the $\xi^r_{\alpha v_\alpha l_\alpha E}$ functions, and it can be split into a delta function term and a principal value term. In applying Eqs. (2) and (5), we have excluded the bound electronic states because contributions from the latter to the ionization process are expected to be negligible.

The resonant wave functions ϕ_r were obtained by diagonalizing the H_2 Hamiltonian in a basis of $\simeq$200 configurations built from B-spline functions of order eight defined in a box of 60 a.u. and with angular momenta up to $l_{\rm max} = 11$ (see [10] for details). Here we consider only the lowest Q_2 $^1\Pi_u$ doubly excited state because it has the largest autoionization width of the series. This state lies above the $^2\Sigma_u^+(2p\sigma_u)$ ionization threshold at $R \geq 1.35$ a.u. At shorter R, the energy curve crosses the threshold and, therefore, the state can decay only to the lowest state of H_2^+ (see Fig. 1). The nonresonant wave functions $\psi^{0+}_{\alpha l_\alpha \epsilon_\alpha}$ describe a bound electron in either the $1s\sigma_g$ or $2p\sigma_u$ orbitals of H_2^+ and a continuum electron with angular momentum up to $l = 7$. They were evaluated using the "L^2 close-coupling" method, which allows for interchannel coupling between different partial waves and yields the correct asymptotic behavior [10]. The ground state of H_2 has been taken from [5]. The initial and final vibrational states have been obtained by diagonalizing the corresponding vibrational Schrödinger equations in a basis of B-spline functions of order eight defined in a box of 12 a.u. Finally, the $\xi^r_{\alpha l_\alpha v_\alpha E}$ wave functions have been obtained by solving Eq. (5) as described in [5].

We show in Fig. 2 the calculated KED spectra for the $^1\Pi_u$ continuum. These are compared with the spectra measured by Ito, Hall, and Ukai [4] for protons observed at 90° with respect to the polarization vector of the incident radiation (note that for this observation angle, only the $^1\Pi_u$ continuum is populated). Since the measurements are not given in an absolute scale, the experimental data have been normalized to reproduce the calculated cross section for $\hbar\omega = 34$ eV and a proton kinetic energy of 7 eV. The same normalization constant is used for all photon energies, so that the experimental relative

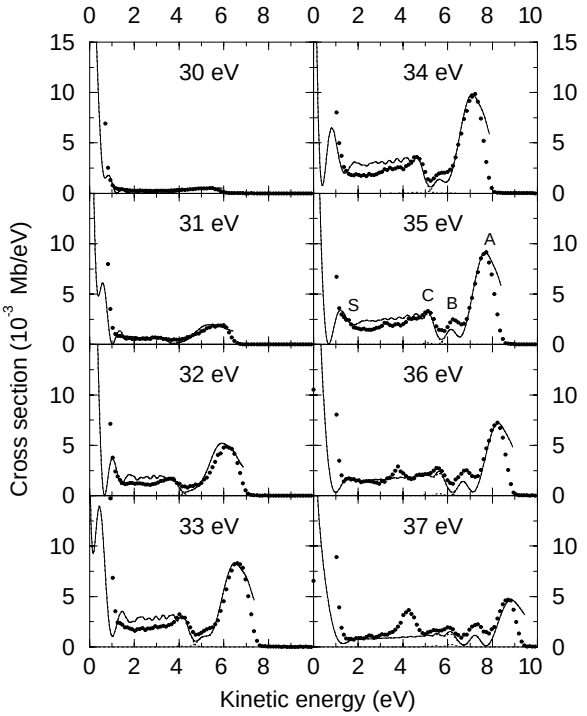

FIG. 2. KED spectra of H_2. Solid line: total cross section; dotted lines: partial cross sections; circles: experimental results from Ref. [4].

intensities remain unchanged. For $\hbar\omega < 36$ eV, the theory reproduces most of the features observed in [4]: peaks *A*, *B*, and *C*, their positions, and relative intensities. In contrast, only peak *A* is present in the experiment of Latimer *et al.* [6]. All the peaks arise from the single doubly excited state $Q_2\ 1^1\Pi_u$. In Ref. [4], peak *B* was attributed to a higher doubly excited state; however, our results show that this interpretation is probably incorrect. Although a contribution from other Q_2 resonances cannot be totally excluded, it should be less important since they lie higher in energy and their autoionization widths are much smaller (e.g., the width of the second $Q_2\ ^1\Pi_u$ resonance is already 10 times smaller at the equilibrium distance $R_e = 1.4$ a.u. [10,11]).

The partial cross sections for dissociation through the $^2\Sigma_g^+(1s\sigma_g)$ and $^2\Sigma_u^+(2p\sigma_u)$ channels are shown as dashed lines in Fig. 2; they can hardly be distinguished from the total cross sections because they contribute in two separate regions of the spectra. The $^2\Sigma_u^+(2p\sigma_u)$ cross section leads to peaks *A* and *B* at high kinetic energy (KE) and is practically zero at smaller KE (e.g., it is negligible below $\simeq$5 eV in the spectrum at 34 eV). The $^2\Sigma_g^+(1s\sigma_g)$ cross section is responsible for the remaining structures, and it is negligible in the region where peaks *A* and *B* appear. Peaks *A* and *B* arise from the resonant terms in the $^2\Sigma_u^+(2p\sigma_u)$ channel [first and third terms on the right-hand side (rhs) of Eq. (2)]; the nonresonant background [the second term on the rhs of Eq. (2)] is very small and barely contributes to the spectra. Peak *C* comes from the resonant terms in the $^2\Sigma_g^+(1s\sigma_g)$ channel. The nonresonant background is responsible for the rapid decay of the cross section from zero to $\simeq$1.5 eV. In this interval one can see a strong oscillation (denoted S) whose shape depends strongly on photon energy. This oscillation is the result of the interference between the resonant and the nonresonant amplitudes. Although the experiments are not conclusive for KE $<$ 1.5 eV, the oscillation has been clearly observed at smaller photon energies ($\hbar\omega <$ 30 eV) [4] and its origin has been discussed in detail in Ref. [5]. Peaks *A*, *B* [channel $^2\Sigma_u^+(2p\sigma_u)$], and *C* [channel $^2\Sigma_g^+(1s\sigma_g)$] are related to autoionization of the $Q_2\ 1^1\Pi_u$ state at three different internuclear distances R_i. These can be approximately determined from the formula [4]

$$2T_i = \{\hbar\omega - [E_r(R_i) - E_\alpha(R_i)] - 18.08\}, \quad (6)$$

where T_i and $[E_r(R_i) - E_\alpha(R_i)]$ are the kinetic energies of the ejected proton and electron, respectively. T_i is directly obtained from the position of maximum i. For peak *A* we obtain that R_A varies from 1.8 to 1.6 a.u. in the photon energy range 30–37 eV. This means that autoionization occurs immediately after the doubly excited state is populated. This is consistent with the fact that the corresponding partial autoionization width (see Fig. 3) is maximum at $R = 1.35$ a.u. Figure 4 shows that the cross section at the maximum position is proportional to the Franck-Condon (FC) factor $|\langle\chi_\nu|\Upsilon_E\rangle|^2$, where Υ_E is the nuclear wave function that results from the equation

$$[E - E_r(R) - T(R)]\Upsilon_E^r(R) = 0. \quad (7)$$

The maximum intensity is obtained for $\hbar\omega = 34.2$ eV, in good agreement with experiments. Notice that Eq. (7) can be easily solved and results from neglecting the autoionizing character of the resonance in Eq. (5). Therefore, the mechanism leading to peak *A* is very simple and can be summarized as follows: (i) the resonance is populated according to the Franck-Condon principle, (ii) the molecule

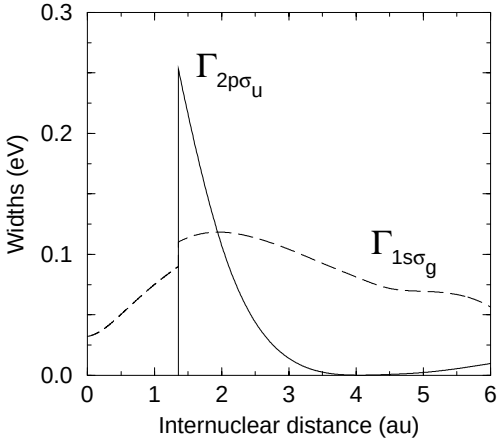

FIG. 3. Partial autoionization widths Γ of the $Q_2\ 1^1\Pi_u$ state. Notice that $\Gamma_{2p\sigma_u}$ is zero when the resonance lies below the $^2\Sigma_u^+(2p\sigma_u)$ threshold.

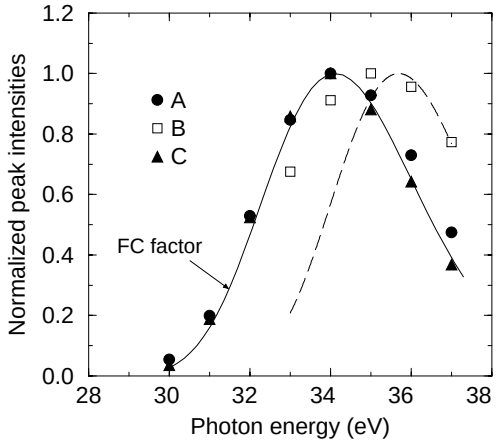

FIG. 4. Peak intensities as functions of photon energy. Solid line: Franck-Condon factor $|\langle\chi_\nu|\Upsilon_E\rangle|^2$; dashed line: $|\langle\chi_\nu|\Upsilon_E\rangle|^2|\langle\chi_{v_\alpha}|\Upsilon_E\rangle|^2$ (see text). All intensities are normalized to 1 at the maximum position.

begins dissociation following the repulsive potential energy curve of the $Q_2\ 1^1\Pi_u$ resonance, (iii) the resonance autoionizes at R_A, and (iv) the molecule dissociates completely following the $^2\Sigma_u^+(2p\sigma_u)$ potential energy curve. Figure 4 shows that peak C exhibits a FC behavior as well; hence the mechanism is similar, except that now dissociation follows the $^2\Sigma_g^+(1s\sigma_g)$ curve in step (iv). From Eq. (6), we obtain $R_C > 7$ a.u., but the existence of a near plateau on the left side of peak C indicates that autoionization occurs, in fact, in the interval $[R_e, R_C]$. This is a consequence of the slow decrease of the $^2\Sigma_g^+(1s\sigma_g)$ partial width with R (see Fig. 3).

We turn now to peak B. From Eq. (6), we obtain $R_B = 2.7 - 2.6$ a.u., which is significantly larger than R_A. Furthermore, the intensity of peak B is not proportional to the Franck-Condon factor $|\langle\chi_\nu|\Upsilon_E\rangle|^2$—Fig. 4 shows that the largest intensity occurs now at $\hbar\omega > 35$ eV. To understand the origin of this unusual behavior one has to analyze the $\xi^r_{\alpha v_\alpha l_\alpha E}$ function resulting from Eq. (2). Since this function combines all dissociation pathways, a second mechanism is possible: (i) The photon populates initially the electronic continuum associated with the $^2\Sigma_u^+(2p\sigma_u)$ state—this step is more or less independent of photon energy; (ii) the molecule begins dissociation following the $^2\Sigma_u^+(2p\sigma_u)$ energy curve; (iii) the resonance is populated at $\simeq R_A$ due to coupling with the electronic continuum—i.e., the inverse of autoionization induced by the inhomogeneous term in Eq. (5); (iv) the resonance autoionizes at R_B; and (v) the molecule dissociates completely following the $^2\Sigma_u^+(2p\sigma_u)$ energy curve. From step (iii), the probability of this second mechanism is roughly proportional to $|\langle\chi_{v_\alpha}|\Upsilon_E\rangle|^2$ [notice that χ_{v_α} is the solution of (4) for $\alpha \equiv {}^2\Sigma_u^+(2p\sigma_u)$]. Since this mechanism interferes with the direct mechanism discussed above, the intensity of peak B should be proportional to $|\langle\chi_\nu|\Upsilon_E\rangle|^2|\langle\chi_{v_\alpha}|\Upsilon_E\rangle|^2$. This leads to the curve shown in Fig. 4, which qualitatively explains the non-Franck-Condon behavior of peak B. Mechanisms involving more steps are less probable because the $^2\Sigma_u^+(2p\sigma_u)$ autoionization width is practically zero for $R > R_B$.

In conclusion, we have presented the first theoretical calculations of resonant dissociative photoionization of H_2 when several autoionization channels are open. We have shown that the resonance structures observed in the 90° KED spectra of H_2 are due to autoionization of a single doubly excited state, $Q_2\ 1^1\Pi_u$, to the $^2\Sigma_g^+(1s\sigma_g)$ and $^2\Sigma_u^+(2p\sigma_u)$ states of H_2^+. At least two different mechanisms are responsible for the various peaks observed in each dissociation channel: a direct (Franck-Condon) mechanism and a multistep (non-Franck-Condon) mechanism. The direct mechanism leads to the most intense peak in each dissociation channel, while the multistep mechanism leads to less intense peaks (the number of which depends on how fast the partial widths decrease at long R). Although these findings provide a simple interpretation of the experimental observations, they do not solve the H_2 problem completely. Indeed, the higher the photon energy, the more ionization channels are accessible, which may explain the presence of the 4 eV peak in the 37 eV spectrum not reproduced by the present calculations (see Fig. 2). Surprisingly, the spectra measured at even higher energies do not show additional structures [4,6]. Therefore, theoretical treatments including more excited channels are necessary in order to clarify the situation. Also, experimental determination of partial cross sections would be highly desirable.

We are grateful to Professor K. Ito for sending us the experimental data. This work has been supported by the DGICYT (PB96-0056).

[1] S. Strathdee and R. Browning, J. Phys. B **12**, 1789 (1979).
[2] K. Kirby, T. Uzer, A. C. Allison, and A. Dalgarno, J. Chem. Phys. **75**, 2820 (1981).
[3] C. J. Latimer *et al.*, J. Phys. B **26**, L595 (1993); J. Geddes *et al.*, *ibid.* **27**, 2961 (1994); Z. X. He *et al.*, J. Chem. Phys. **103**, 3912 (1995).
[4] K. Ito, R. I. Hall, and M. Ukai, J. Chem. Phys. **104**, 8449 (1996).
[5] I. Sánchez and F. Martín, Phys. Rev. Lett. **79**, 1654 (1997); Phys. Rev. A **57**, 1006 (1998).
[6] C. J. Latimer *et al.*, J. Phys. B **29**, 6113 (1996).
[7] J. N. Bardsley, J. Phys. B **1**, 349 (1968).
[8] A. U. Hazi, T. N. Rescigno, and M. Kurilla, Phys. Rev. A **23**, 1089 (1981).
[9] C. de Boor, *A Practical Guide to Splines* (Springer, New York, 1978).
[10] I. Sánchez and F. Martín, J. Chem. Phys. **106**, 7720 (1997); **110**, 6702 (1999).
[11] J. Tennyson, At. Data Nucl. Data Tables **64**, 253 (1996).